PCCP

Accepted Manuscript

ROYAL SOCIETY OF CHEMISTRY

www.rsc.org/pccp

Electronic Coupling between Ligand and Core Energy States in Dithiolate-Monothiolate Stabilized Au Clusters

Tarushee Ahuja,[§] Dengchao Wang,[§] Zhenghua Tang,[¥] Donald A. Robinson,[†] Jonathan Padelford and Gangli Wang*

Department of Chemistry, Georgia State University, Atlanta, Georgia 30302

Supporting Information Placeholder

ABSTRACT: Electron transfer activities of metal clusters are fundamentally significant and have promising potentials in catalysis, charge or energy storage, sensing, biomedical and other applications. Strong resonance coupling between the metal core energy states and ligand molecular orbitals has not been established experimentally, albeit exciting progresses have been achieved in the composition and structure determinations of these types of nanomaterials recently. In this report, the coupling between core and ligand energy states is demonstrated by the rich electron transfer activities of Au_{130} clusters. Quantized electron transfers to the core and multi-electron transfers involving the durene-dithiolate ligands were observed at lower and higher potentials respectively in voltammetric studies. After a facile multi-electron oxidation at + 1.34 ~ + 1.40 V, several reversal reduction processes at more negative potentials, i.e. +0.91 V, +0.18 V and -0.34 V, were observed in an electrochemically irreversible fashion, or sluggish kinetics. The number of electrons and the shifts of the respective reduction potentials in the reversal process were attributed to the electronic coupling or energy relaxation processes. The electron transfer activities and subsequent relaxation processes are drastically reduced at lower temperatures. The time and temperature dependent relaxation, involving multiple energy states in the reversal reduction processes upon the oxidation of ligands, reveals the coupling between core and ligand energy states.

INTRODUCTION

Metal clusters have attracted extensive research interest in nanoscience, classic inorganic chemistry and electrochemistry due to their rich and tunable electrochemical, optical and other properties. Gold nanoclusters stabilized by a monolayer of thiolate ligands[1] gained extensive research attentions recently primarily for two reasons: the discovery of a unique thiol bridging (RS-Au-SR) motif at the core-ligand interface,[2] and the elucidation of atomic/molecular compositions.[3] The information could potentially enable definitive structure-function correlation, which is an important question that challenges broadly defined nanomaterials research. The extraordinary stability of the Au nanoclusters, facile synthesis and isolation, and readily tunable properties make them excellent prototype systems and promising candidates to establish this fundamentally significant concept for broad applications.[4]

Controlled resonance coupling between the metal core energetics and ligand energy states has not been established experimentally. Such electronic coupling could add another dimension to tailor the properties of these functional metal clusters. The rationale is rooted on ligand-metal charge transfer, a widely adopted concept in classic inorganic chemistry. The charge density shift via electron resonance between metal ion center and ligand orbitals are often accompanied with changes in absorption, luminescence and electrochemistry activities. Similarly, new properties could emerge from the electronic coupling between the core and the capping ligands of the gold nanoclusters or other nanomaterials.[1]

Two criteria are believed keys to achieve and to manifest the electronic coupling: 1. metal cores with well-defined energetics and 2. proper linkers between the metal core and the structure of the ligand molecules that have accessible orbitals. Inert ligands are typically employed serving the primary function to stabilize the metal cores.[5] Correspondingly, the ligands themselves, excluding the sulfur atoms that bound with Au core, are generally believed to have negligible contributions to the overall energetics of Au nanoclusters.[6] Ligands with accessible energy states, such as electroactive molecules as redox probes, have been introduced as part of the ligands to a variety of nanoparticles, especially with Au nanoclusters.[7] Albeit multi-electron transfer activities have been observed corresponding to those redox molecules, the impact by the nanoparticles on the electrochemical potential of the redox probe was unremarkable as pointed out in Murray's review.[1a] The observation suggests negligible electronic coupling between the nanocore energetics (Au and S)[6] and the molecular orbitals of the redox probes, often at the outer surface separated from the Au-thiolate interface by the linker portion of the ligands.

The energetics of Au nanoclusters is routinely characterized by electrochemical and optical methods. [1a, 8] Multiple electron transfer peaks separated by relatively uniform charging energy have been observed over wide potential range in voltammetric studies from Au nanoclusters with relatively larger cores (i.e. Au_{130} and $Au_{140-147}$).[9] Each peak represents single electron transfer activity, which is well-known as quantized double-layer (QDL) charging or Columbic staircase behaviors. The absorption spectra generally display a featureless decay from UV to visible and near IR range. For those Au nanoclusters with relatively smaller core size (i.e. Au_{13}, Au_{25}, Au_{38}, Au_{55} and Au_{75}),

molecular-level energy states emerge in voltammograms that can be correlated with the discrete absorption bands in UV-visible spectra.[10] The experimental energy diagrams and structural information of several Au nanocluster systems are often employed to validate and to gain fundamental insights from density function theory calculations.[6, 11] The contribution of the ligands to the overall nanoclusters energetics is primarily evaluated by Au-S bonding, i.e. in superatom theory.[6]

In this report, strong coupling between the Au core and ligand energy states is evidenced for the first time by multiple electrochemical techniques. Electronic transitions involving both Au_{130}[12] nanocores and the stabilizing durene-dithiolate ligands and their interplay are quantified. Scan-rate dependent cyclic voltammograms reveal single electron transfer QDL charging behaviors at lower potentials; while single-step multiple electron transfers (ETs) involving ligand energy states are observed at higher potentials. The relaxation involving chemical transformation after the multi-ET ligand oxidation in the reversal potential scans is further characterized by normal pulse voltammetry and chronoamperometry. The ET coefficients at different energy states are quantified.

EXPERIMENTAL

Chemicals. Tetrachloroauric acid trihydrate ($HAuCl_4 \cdot 3H_2O$, >99.99%), 2-phenylethanethiol (PET, >99%), tetraoctylammonium bromide (TOABr, 98%), sodium borohydride ($NaBH_4$, 99%), tetrabutylammonium perchlorate (TBAP, >99%), and all other solvent (HPLC grade) including toluene, methanol and CH_2Cl_2 were all used as received from Sigma-Aldrich. Durene-□1, □2-dithiol (Durene-DT, >95%) was obtained from TCI-America.

Instruments. The UV-vis absorbance spectrum was recorded with Shimadzu UV-1700 spectrophotometer. MALDI mass spectra were collected with ABI 4800 matrix assisted laser desorption ionization (MALDI) TOF-TOF analyzer. A CH instrument 700C electrochemical workstation was used in electrochemical measurements.

Au_{130}(Durene-DT)$_{29}$(PET)$_{22}$ synthesis and characterization. The synthesis and purification procedure of Au_{130} nanoclusters mainly follow previous reports.[12] Briefly, the gold salt ($HAuCl_4 \cdot 3H_2O$) was first phase-transferred into toluene with TOABr, followed by adding in a mixed Durene-DT/PET solution under stirring, and the final ratio of Au/Durene-DT/PET is 1.5:1:2. Then freshly prepared $NaBH_4$ (20 equiv. of gold) aqueous solution was added. After 3 days, the organic layer was separated and washed with water and then precipitated by methanol. The Au_{130} nanoclusters composition was confirmed by the UV-vis and MALDI (Figure SI-1 and SI-2) following previously described analysis. The 3-nm Au plasmonic nanoparticles were synthesized and purified similarly, but with Au:Durene-DT ratio at 1:1 prior to reduction.

Electrochemistry. All the electrochemical tests were conducted in CH_2Cl_2 solvent containing 0.1 M TBAP as supporting electrolyte, and all the solutions are purged with Argon gas for 20 min prior to testing. The Au_{130} nanocluster concentration is around 0.1 mM. The working electrode was a 0.24 mm-radius Pt disk electrode. Before use, this Pt electrode was polished with alumina oxide powder, washed and sonicated with water, acetone and CH_2Cl_2. The counter electrode was Pt foil, and Ag/AgCl wire was used as quasi-reference electrode (QRE). The potential of the AgQRE (0.22 V vs. SHE) was calibrated by measuring the ferrocene (Fc^+/Fc) redox peak at 0.48 V.

RESULTS AND DISCUSSION

Core charging and discharging. At least six consecutive single electron transfer processes can be resolved within a narrow potential range, from ca. -0.8 V to + 0.4 V, in the cyclic voltammograms at different scan rates shown in Figure 1A. This should not be confused with those by pulse analysis, such as the square wave voltammetry (SWV) features shown in panel B (four uniform spacing shown) and those by differential pulse voltammetry (DPV) in literature, that are routinely employed to better resolve the peak position. The discrete peaks directly from cyclic voltammetry (CV) indicate high monodispersity of the sample and allow quantitative and mechanistic diagnosis discussed next.

The uniform spacing of the QDL peaks is 0.21±0.01 V, which corresponds to the charging energy of individual electrons transferred to the same energy states (inner Au core plus Au-S interface). A capacitance of $C = e/\Delta V = 0.76$ aF is determined accordingly. This charging energy is significantly lower than the 0.26 eV observed from the well-studied $Au_{140\text{-}147}$ clusters stabilized by hexane thiolates.[9a, 9b] Based on the concentric sphere model ($C = 4\pi\varepsilon R(R+d)/d$), and given the similarity in Au core sizes (R), the larger capacitance is attributed to the lower dielectric constant (ε) and thinner thickness (d) of the monolayer arising from the aromatic ligand molecular structures (Durene-DT and PET). Another pair of peaks is separated by a ca. 0.36±0.01 V gap upon further oxidation around +0.40 V (panel B). Because the open circuit potential of the Au_{130} clusters is typically near 0 V, this pair of charging peaks in both oxidation and reduction scans reveal a discrete energy state that is slightly below the degenerated frontier orbitals/states, i.e. HOMO, instead of a HOMO-LUMO gap. Regardless, this 0.36 V gap is another feature not observed from the well-studied $Au_{140\text{-}146}$ clusters in which the QDL peaks are relatively symmetric around frontier states.[9a, 9b] The large spacing cannot be explained by counter ion penetration (or polar solvent) into the ligand monolayer, which is known to increase the dielectric constant ε and thus decrease the charging energy.[13]

At higher potential scan rates, the peak current increases while the peak positions remain largely unchanged, with ca. 59 mV peak separation between the forward and backward scans. The observations suggest diffusion-limited processes, or facile (electrochemical reversible) and chemically reversible ET processes. The overall ET features within this narrow potential range are reminiscent of the continuous QDL charging behavior observed for larger Au nanoclusters composed of 140 or more total Au atoms.[9a, 9b] The continuous energy states are supported by the similar inner core structures containing 105-Au atom in truncated-dodecahedral geometry resolved recently through combined electron diffraction scanning TEM measurements and DFT calculations.[9e, 14]

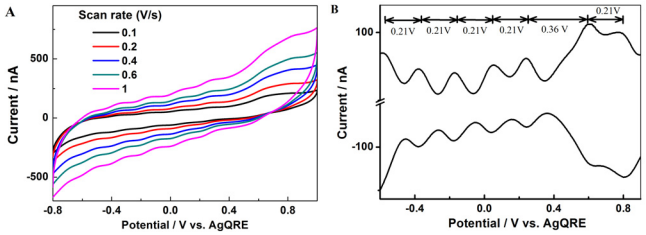

Figure 1. **A:** cyclic voltammograms and **B:** square wave voltammograms (SWVs) of ~0.1 mM Au_{130} nanoclusters in CH_2Cl_2 with 0.1 M TBAP as supporting electrolyte. The SWVs were obtained with 25 mV amplitude, an increment of 4 mV and the frequency is 15 Hz. Peak spacing is listed in panel B.

Oxidation of ligands. At higher potential amplitudes, ca. + 1.34 V, large anionic peaks were recorded at different scan rates shown in Figure 2. Because this oxidation process is not observed from other Au-thiolate clusters especially those with PET ligands, simple dissociative oxidation at Au-S bonding interface is ruled out. The multi-electron oxidation processes have been attributed to the radical formation involving Durene-DT ligands.[15] For reference, the voltammogram of Durene-DT, albeit adsorptive on electrode surface, is included in Figure SI-3 to demonstrate the corresponding oxidation processes. It is worth pointing out that the reversal reduction is largely featureless, particularly compared to those at +0.91V, +0.18V and -0.34V as observed in Au clusters. This notion is important in the discussion of electron relaxation and coupling processes. The durene-dithiol is very different from monothiols such as phenylethanethiol. The oxidized form of Durene-DT could readily form a heterocyclic six-membered disulfide ring that is highly adsorptive on electrode. The intra-molecule disulfide will be more thermodynamically and kinetically favored over monothiols. Therefore, the durent-DT ligands on Au clusters should not be confused with durene (no thiol groups), durene-dithiols in solution, and monothiolate ligands in terms of radical stability or reactivity with environment. Because the peak current at 1.34 V is proportional to the cluster concentration (results not shown), possible impacts by, i.e. trace amount of impurities, are ruled out. The QDL peaks at lower potentials are less distinct visually due to the large current involving the ligands.

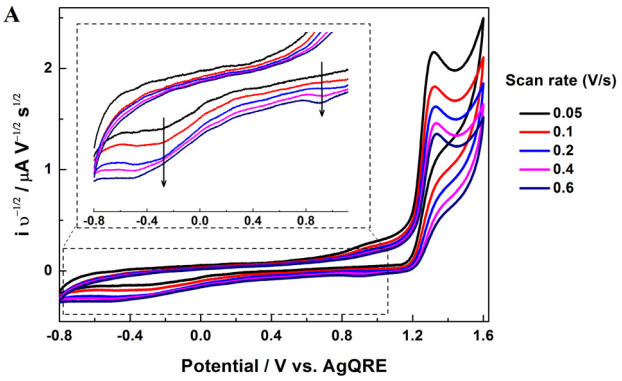

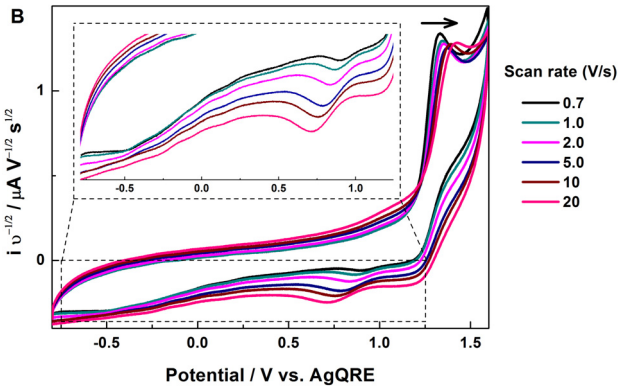

Figure 2. **A:** CVs including Durene-DT ligand oxidation under relatively slow scan rates of 0.05, 0.1, 0.2, 0.4 and 0.6 V/s. Arrows in the inset indicate the increase in scan rates. **B:** CVs at fast scan rate of 0.7, 1, 2, 5, 10 and 20 V/s. The arrow indicates the shift in peak potential. The current was normalized by the square root of the scan rates. Reversal reduction processes are zoomed in as an inset.

The oxidation peak at +1.34 V displays characteristics of facile ET followed by a chemical reaction at lower scan rates shown in Figure 2 panel A. Note the current is already divided by the square root of the scan rates ($\upsilon^{1/2}$) to normalize the diffusion contribution. In reference to the single ET QDL current, the large current reflects multiple ET activities quantified next. The peak potential is insensitive to scan rates while the peak shape is non-broadened and can be fitted by one-electron kinetics, which suggest multiple electrons transferred to individual non-interacting orbitals. The argument is supported by earlier analysis of conductive polymers and Au clusters functionalized with non-interacting redox centers such as ferrocene.[7c, 16] Albeit the peak shape and peak potential remain unaffected, $i/\upsilon^{1/2}$ is found to decrease at higher scan rates, indicating a follow-up chemical reaction mechanism after the multi-ET oxidation. At even higher scan rates, the peak potential shifts to more positive shown in panel B. Apparently the ET responses become quasi-reversible (relatively sluggish) under faster perturbation. The increase in peak current at extreme high scan rates is due to the superimposed capacitive charging current at electrode/solution interface, which is proportional to υ instead of $\upsilon^{1/2}$. A dissociative reaction mechanism in the reduction of Au_{25} clusters has been reported by Maran's group.[17] The stripping of thiolate ligands makes the process chemically irreversible. In this report, the potential is limited in the reduction scan to avoid such stability concerns.

Reversal reductions after ligand oxidation. New cathodic processes emerge in the reversal reduction superimposed on QDL current that spreads over the whole potential range. Next we focus on those reduction features only observable after the ligand is oxidized. At lower scan rates (Figure 2A inset), additional reduction currents were captured at drastically shifted and broad reduction potentials (-0.4 to 0 V), arising around 0 V and approached a plateau around –0.4 V. The significant decrease in current amplitude compared to the +1.34 V oxidation can be explained by the mass transport loss and possible chemical/structural changes of the oxidized products when scanned to those potentials. Another discrete reduction peak around +0.9 V becomes more prominent at higher scan rates (panel B

inset). The +0.9 V peak shifts toward less positive, suggesting a diffusive quasi to irreversible ET process. Interestingly, relative to the increase in the +0.9 V peak current at higher scan rates, the broad reduction features at -0.4 to 0 V become less defined and diminish into baseline current. The +0.9V peak becomes distinguishable at 0.4 V/s scan rate, which suggest a lifetime of up to 2 s of the corresponding species (the calculation is described in supporting information).

The correlation of those ET processes suggest that the energy states or orbitals at +0.9 V could be filled by the electron relaxations from higher energy states (-0.4 to 0 V) at the time scale of seconds. In other words, after the facile ligand oxidation, the relative changes in the two reduction processes reveal the conversion between one more stable (longer life time) oxidized species (-0.4 to 0 V) and another shorter lived ones (+0.9 V).

Next, to better resolve those electron coupling/relaxation activities, normal pulse voltammetry (NPV) was employed with the results shown in Figure 3. (The advantages of NPV to analyze this system is explained in supporting information)

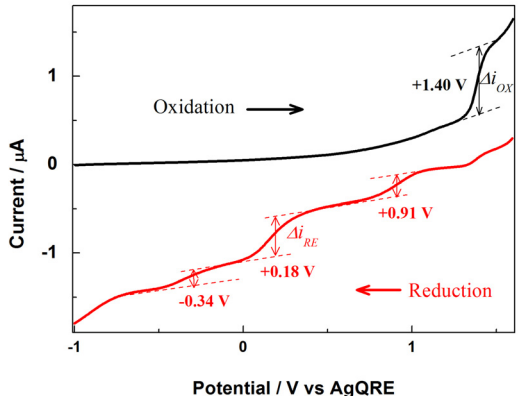

Figure 3. Normal Pulse Voltammograms (NPVs) of Au_{130} nanoclusters in CH_2Cl_2 with 0.1 M TBAP. The measurement parameters are: 0.05 V pulse width, 16.7 ms sample width, 0.2 s pulse period, 4 mV potential increment. Three distinct peaks, +0.91, +0.18 and -0.34 V are observed in the reduction process. The sample width (16.7 ms) corresponds to high scan rates in the CV measurements so that the oxidation potential (+ 1.40 V) is slightly larger than +1.34 V as observed in CVs.

The reduction curve was collected at an initial potential of +1.60 V, sufficiently more positive than the +1.34 V to replenish the oxidized species within the diffuse layer at each potential step. Three main reduction processes centered at +0.91 V, +0.18 V and -0.34 V can be resolved. Based on the current ratio ($\Delta i_{Red}/\Delta i_{Ox}$) at each reduction potential with respect to the oxidation current, about 37%, 53% and 18 % of the total oxidation products are reduced at those three potentials respectively. It is worth mentioning that a weak shoulder around +0.9 exists in the oxidation scans in both CVs and NPVs. With current recorded at 0.0167 s after each potential step, the loss of oxidation products is obviously less significant compared to CVs. It is interesting to notice that the total reduction current (from +1.0 V to -0.8/-0.4 V) matches nicely with the total oxidation current (+ 1.40 V).

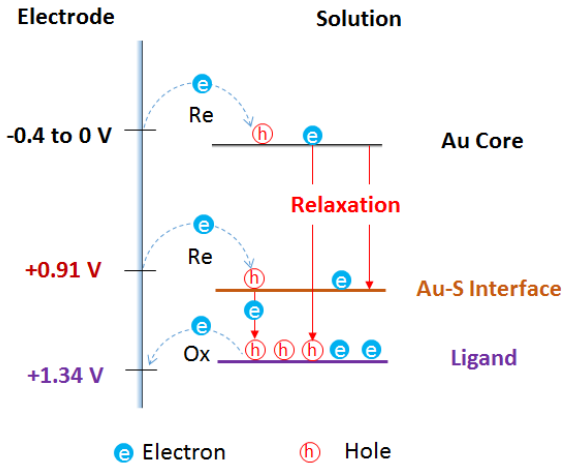

Scheme 1. Diagram of the electron relaxation processes after ligand oxidation.

Taken together, we propose an electron relaxation mechanism illustrated in Scheme 1. Because we are studying dynamic ET processes, the two electrons constituting the Au-S bonding should not be perceived the same as those delocalized in Au core energy states: they are more localized. After the oxidation at +1.34 V, those newly-emptied non-interacting ligand orbitals can be filled by the delocalized electrons in the Au_{130} core and those involved in Au-S bonding at higher energy states, -0.4 to 0 V and +0.9 V respectively. The two relaxation processes clearly display different time constants. The cationic radicals are stabilized by two factors in these clusters: the electron-rich sulfur and the hydrophobic aromatic ring on the periphery. Under fast potential scan rates in CVs or direct potential stepping in NPVs, multi electron reduction can be detected at a non-spread potential around +0.91 V. The reduction by electrode fills those non-interacting Au-S bonding orbitals after the original electrons relax into the vacant + 1.34 V states. If the reversal reductions were captured at a larger time scale, such as slow potential scan rates, the +0.9 V reduction peak disappears while reduction at potential ranges around -0.4 to 0 V becomes more prominent. This clearly suggests that the electrons in the Au_{130} core (-0.4 to 0 V) will also gradually relax into and fill the Au-S interface orbitals (+0.9 V), therefore no reduction peaks can be observed at +0.9 V with scan rates lower than 0.4 V/s (Figure 2A). It is worth mentioning that the electron relaxation from core to ligand energy states do not change the overall charge of the Au clusters, therefore should not induce counter ion reorganization. The sluggish kinetics and long lifetime is hypothesized to be the result of chemical transformations after ET oxidation such as core structural changes or ligand radical reactions that require further experimental and theoretical characterizations.

With the three distinct reduction processes at -0.34, +0.18 and +0.91 V resolved by NPVs, potential step chronoamperometry was performed to capture the transient relaxation processes. After applying +1.6 V for 2 s to produce reproducible amount of oxidized products, the potential was stepped to -0.5, 0.0, and +0.7 V respectively (a small over potential was added in each measurement to ensure the current responses are determined by the diffusion process rather than electrode kinetics). Figure 4 shows those i-t and $i\text{-}t^{-1/2}$ curves at different potentials. For pure diffusion-limited responses, a linear relationship is

expected in the $i\text{-}t^{-1/2}$ curve, in which the number of transferred electrons can be determined from the slope based on the Cottrell equation. A step to + 0.7 V will measure electrons needed to fill those vacant orbitals accessible, i.e. the + 0.91 V ones. At -0.5 V, the current will include all three reduction processes. An important observation in Figure 3 is that, at larger time scale (1 to 2 s), the slope at 0.7 V decreases more significantly compared to the slope/curvature at -0.5 and 0 V, suggesting the +0.9 V states becoming inaccessible, already filled by a slower relaxation process from orbitals with higher energy states (-0.4 to 0 V) to +0.9 V orbitals.

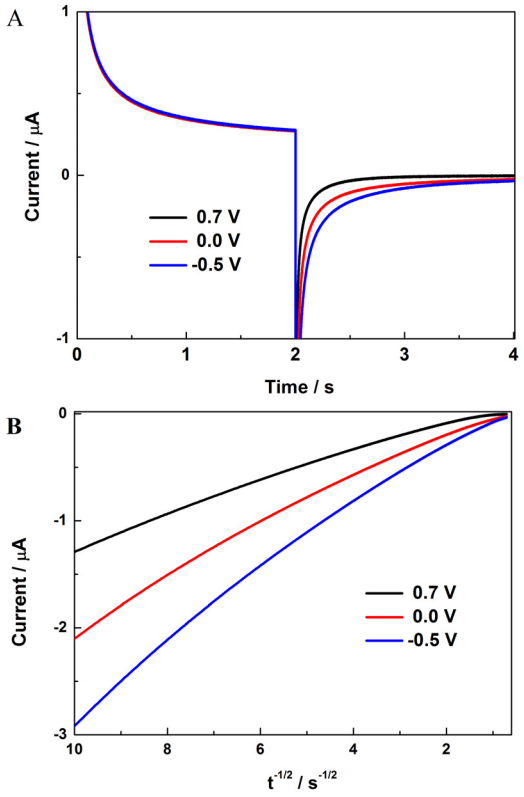

Figure 4. A: Potential-step current-time curves from the same initial +1.60 V (0-2 seconds) to different end potentials 0.7, 0.0 and -0.5 V (2-4 s). **B:** Cottrell plots of the reversal reducitons from 0.01 to 2 s respectively. Data below 10 ms was not included due to the charging effect (RC time constant is ca. 2-3 ms).The sampling interval is 0.1 ms.

Data analysis and linear fitting of the Cottrell curves at different time periods are detailed in Figure SI-4. Within 0.01 to 0.05 s, more than 97 % of those oxidized species was reduced at – 0.5 V. This impressive number suggests almost full recovery or chemical reversibility. Among this 97%, 46% was captured at the + 0.7 V reduction, which leave 25% to the 0.0 V reduction and another 26% to the – 0.5 V reduction. In other words, about 50% of the vacant orbitals by the + 1.34 oxidation is filled within 10 ms by the electron relaxation from + 0.9 V states, 25% by those from + 0.18 V states, and another 25% by the -0.34 V states. At longer time, possible processes such as core structural changes, radical reactions involving durene-DT[15] as well as mass transport loss cause the slope to further decrease in all three curves. Normalized by the slope of the – 0.5 V curve under the assumption of it accounts for the total oxidized states/species still accessible by the electrode, the slope of the + 0.7 V curve decreases to 44% (36%/82%) within 0.2-0.4 s and 14% (8/58%) within 1-2 s respectively. Because other possible losses have been normalized, the decrease accounts for the electrons relaxed from higher energy states, i.e. frontier states around +0.18 V and -0.34 V. The difference in the 0.0 V and -0.5 V curvatures is minimal over different time scale, probably corresponding to broad frontier states whose degeneracy could be changed during these processes that requires further analysis. Apparently, the electron relaxation from those frontier states into the +0.9 V states is gradual with a lifetime about 2 s, which agrees well with the scan rate CV analysis. Further, the electron relaxation occurs at a single potential (CA and NPV), which is consistent with the non-broadened +0.9 V peak shape in CV, attesting the assignments of relaxation into non-interacting states, i.e. those localized as Au-S-Durene bonding. It is unclear at this point if those states also involve the rest Durene-DT ligand molecular structures or solely the Au-S bonding.

Quantification of ETs. It is nontrivial to quantify the number of ET due to the time-dependent relaxation. The results from multiple electroanalytical techniques are discussed next. The number of ETs corresponding to ligand oxidation is quantified first. For a diffusion limited facile ET process,

$$i_p = (2.69\times10^5)n^{3/2}AD_0^{1/2}C_0\upsilon^{1/2} \qquad (1)$$

i_p: peak current, n: # of electrons transferred, A: area of working electrode, D_0: diffusion coefficient, C_0: concentration, and υ: scan rate.

As explained in the early theoretical analysis by Flanagan et. al.[16], for multiple electrons transferred to non-interacting redox centers (molecular orbitals), the peak shape remains while the peak current is directly proportional to the number of electrons instead of $n^{3/2}$. Shown in Figure 5A, the oxidation current of one QDL peak at -0.35 V and that of the ligands at +1.34 V is largely linear with square root scan rate, confirming diffusion limited facile ET activities. Because A, D_0 and C_0 are the same, using the well-defined single electron transfer QDL peaks as the reference, the ET number at +1.34 V is calculated to be ~58. While the absolute number of ligand oxidation varies by few from different batches of Au_{130} samples (29 per cluster on average), the results suggest that about two electrons per Durene-DT ligands are oxidized in those ET processes, behaving as redox labels.

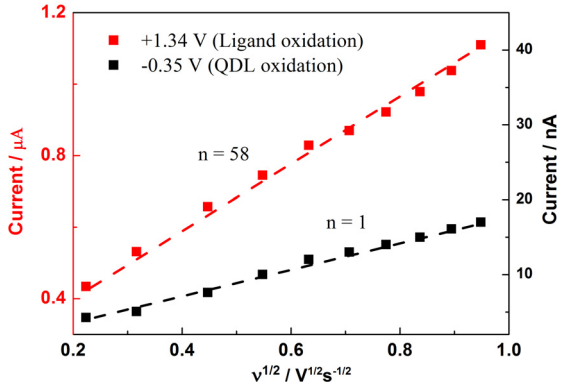

Figure 5. The peak currents vs square root scan rate and their corresponding fitting of the QDL and ligand oxidation peaks at -0.35 and +1.34 V, data are obtained from Figure 1 and 2.

Potential-step chronoamperometry analysis, shown in Figure 4 and Figure SI-4, offers better quantitative analysis of the reversal reduction processes at different time scale. For example, after 59 e oxidation at +1.34 V, within 0.01 to 0.05 s, 27 e from the +0.9 V states will relax into the vacant ligand orbitals, with the rest 30-31 e being filled by the relaxation from the core electrons (i.e. 15 e from -0.34V and another 15 e from +0.18 V). At longer time up to 2 s, 34 e of the 58 e can be reduced directly at – 0.4 V. The 34 e includes 5 e to the +0.9 V, 17 e to the +0.18 V and 12 e to the -0.34 V states. The relative decrease of the +0.9 V reduction with respect to the core energy states reflects those electrons relaxed into lower energy states. The loss of total electrons, 34 out of 58, might be limited by electrokinetic and mass transport loss. Because the main optical absorption peaks and electrochemical peaks remain largely unchanged after repeated CV scans including ligand oxidation (hundreds cycles), possible irreversible processes, such as oxidative stripping of Durene-DT ligands or radical chemical reactions, are believed insignificant, at least at scan rates higher than 0.5 V/s.

The above analysis is also consistent with the CV features of two linear regions at low and high scan rate ranges, with transitions at middle scan rate range, as shown in Figure SI-5. Because CV analysis is relative slow compared to the amperometric analysis and the baseline is greatly affected by the charging currents, only 8 electrons were resolved in the data presented. Regardless, the complement slopes suggest the electron relaxation from the core to Au-S interface states as time progresses (slower scan rates, toward left).

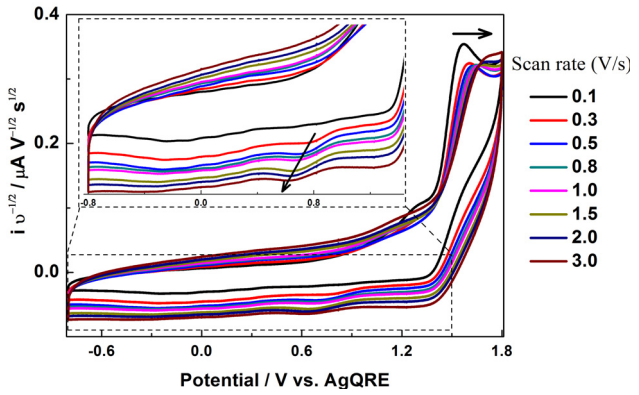

Figure 6. CVs of the Au_{130} nanoclusters at low tempreature (195 K) in CH_2Cl_2 with 0.1 M TBAP as supporting electrolyte. Data were collected in dry ice/ethanol bath.

Temperature dependent relaxation. Next we present the preliminary studies at lower temperature (195 K) of the ligand oxidation and reversal reduction processes to gain further insights and support of the proposed relaxation process. Systematic studies will be reported later for kinetic and thermodynamic discussions. The CV results normalized by the $^{1/2}$ are shown in Figure 6. The oxidation process of the Durene-DT ligand is less reversible compared to that under room tempreature, as the oxidation peak potential shifts more potisitve with the increase in scan rates. In addition to the slower ET kinetics, because the diffusion coefficient decreases at lower temperature, the ligands accessible for ET reactions at the electrode are more restrained by the limited rotational diffusion. Accordingly, only 20 electrons were transferred in the oxidation process based on the peak current ratio over QDL peaks. Compared to the RT behavior, the reversal Au-S reduction at + 0.8 V appears to be more dominant even at very slow scan rates. Additional reduction current around the frontier states, from +0.4 to -0.4 V, is still detectable (in reference to the oxidation curent within the same range corresponding to QDL charging), but less significant compared to RT results. The distorted reversal reduction peaks are indicative of the electronic coupling between the core and ligand energy states, which refute irreversilbe chemical reactions such as ligand stripping: an increase in QDL peak current would not be expected. Overall, the decrease in the electronic coupling/relaxation at low temperature, particularly those from the core frontier states, suggest high possibility of core structure changes or reversible radical chemical transformation during the slow relaxation.

Last but not least, plasmonic Au nanoparticle with 3-nm core diameter[18] stabilized by Durene-DT ligands were tested. Similar voltammetric features were observed as shown in Figure SI-6. Compared to the Au_{130}, the ligands are oxidized at + 1.23 V rather than + 1.34V. Reversal reduction processes, also only observed following ligand oxidation, are shifted to + 0.75 V and – 0.27 V respectively. The less positive potentials suggest stronger stabilization of the oxidized species by the larger core. Because single QDL peaks could not be resolved from large plasmonic nanoparticles due to the small charging energy, the charges in the oxidation and reduction scans were compared. In both without ligand ETs in small potential window and with ligand ETs, the integrated areas as shown in panel C, or charges, compensate in the respective oxidation and reduction scans. The observed multi-ET processes and the shifts in the redox potentials from a different sized Au core provide further evidence of the coupling between the ligand and core energy states.

CONCLUSIONS

In summary, multiple electron relaxation processes at different time scale has been observed in molecule-like Au_{130} nanocluster by different electrochemical techniques. The relaxations from Au core and Au-ligand interface states to the ligand orbitals are observed after the ligand oxidation. At room temperature, up to 58 electrons from the Durene-DT ligands (2e per ligand) are transferred during the ligand oxidation process. Within 10 ms, 27 and 30-31 electrons from the Au-S interface (+0.91 V) and core frontier states (-0.34 V - +0.18 V) will relax and fill in the empty ligand orbits. Meanwhile, the electrons from core frontier will gradually (up to seconds) fill in the Au-S interface states as well. The core frontier states are coupled and display quantized double layer characteristics, while the Au-S interface states are non-interacting. The dynamic relaxation activities clearly reveal the electron coupling between the ligand and core energy states. Furthermore, the decrease in the ET and subsequent relaxation at low temperature suggests possible structure changes during the sluggish electron relaxation process that requires further analysis.

ASSOCIATED CONTENT

Supporting Information. The characterization of the Au_{130} nanoclusters including UV-vis and MALDI; Electrochemistry

behaviors of Durene-DT ligand, and the details of the calculation of transferred electrons. Material is available free of charge via the Internet at http://pubs.acs.org.

AUTHOR INFORMATION

Corresponding Author

*E-mail: glwang@ gsu.edu

§: These authors contributed equally.

Present Addresses

[¥]New Energy Research Institute, School of Environment and Energy, South China University of Technology, Guangzhou Higher Education Mega Center, Guangzhou, China, 510006.
†Department of Chemistry, The University of Texas at Austin, 105 East 24th Street Stop A5300, Austin, Texas 78712-1224, United States.

Notes

The authors declare no competing financial interest.

ACKNOWLEDGMENT

The grant from National Science Foundation (No. 1059022) is gratefully acknowledged. D. W. acknowledges the B&B fellowship.

REFERENCE

1. (a) Murray, R. W. *Chem. Rev.* **2008,** *108*, 2688-2720; (b) Sardar, R.; Funston, A. M.; Mulvaney, P.; Murray, R. W. *Langmuir* **2009,** *25*, 13840-13851; (c) Jin, R. C. *Nanoscale* **2010,** *2*, 343-362; (d) Zheng, J.; Zhou, C.; Yu, M. X.; Liu, J. B. *Nanoscale* **2012,** *4*, 4073-4083.
2. (a) Jadzinsky, P. D.; Calero, G.; Ackerson, C. J.; Bushnell, D. A.; Kornberg, R. D. *Science* **2007,** *318*, 430-433; (b) Heaven, M. W.; Dass, A.; White, P. S.; Holt, K. M.; Murray, R. W. *J. Am. Chem. Soc.* **2008,** *130*, 3754-3755; (c) Zhu, M.; Aikens, C. M.; Hollander, F. J.; Schatz, G. C.; Jin, R. *J. Am. Chem. Soc.* **2008,** *130*, 5883-5885.
3. (a) Dass, A.; Stevenson, A.; Dubay, G. R.; Tracy, J. B.; Murray, R. W. *J. Am. Chem. Soc.* **2008,** *130*, 5940-5946; (b) Tracy, J. B.; Crowe, M. C.; Parker, J. F.; Hampe, O.; Fields-Zinna, C. A.; Dass, A.; Murray, R. W. *J. Am. Chem. Soc.* **2007,** *129*, 16209-16215.
4. (a) Li, G.; Jin, R. C. *Acc. Chem. Res.* **2013,** *46*, 1749-1758; (b) Zhou, C.; Yang, S. Y.; Liu, J. B.; Yu, M. X.; Zheng, J. *Exp. Biol. Med.* **2013,** *238*, 1199-1209.
5. (a) Qian, H. F.; Zhu, M. Z.; Wu, Z. K.; Jin, R. C. *Acc. Chem. Res.* **2012,** *45*, 1470-1479; (b) Templeton, A. C.; Wuelfing, M. P.; Murray, R. W. *Acc. Chem. Res.* **2000,** *33*, 27-36.
6. Walter, M.; Akola, J.; Lopez-Acevedo, O.; Jadzinsky, P. D.; Calero, G.; Ackerson, C. J.; Whetten, R. L.; Gronbeck, H.; Hakkinen, H. *P. Natl. Acad. Sci. U.S.A.* **2008,** *105*, 9157-9162.
7. (a) Li, D.; Zhang, Y. J.; Jiang, J. G.; Li, J. H. *J. Colloid Interf. Sci.* **2003,** *264*, 109-113; (b) Chen, S. W.; Huang, K. *Langmuir* **2000,** *16*, 2014-2018; (c) Wolfe, R. L.; Balasubramanian, R.; Tracy, J. B.; Murray, R. W. *Langmuir* **2007,** *23*, 2247-2254.
8. Laaksonen, T.; Ruiz, V.; Liljeroth, P.; Quinn, B. M. *Chem. Soc. Rev.* **2008,** *37*, 1836-1846.
9. (a) Hicks, J. F.; Miles, D. T.; Murray, R. W. *J. Am. Chem. Soc.* **2002,** *124*, 13322-13328; (b) Quinn, B. M.; Liljeroth, P.; Ruiz, V.; Laaksonen, T.; Kontturi, K. *J. Am. Chem. Soc.* **2003,** *125*, 6644-6645; (c) Jupally, V. R.; Thrasher, J. G.; Dass, A. *Analyst* **2014,** *139*, 1826-1829; (d) Jupally, V. R.; Dass, A. *Phys. Chem. Chem. Phys.* **2014,** *16*, 10473-10479; (e) Negishi, Y.; Sakamoto, C.; Ohyama, T.; Tsukuda, T. *J. Phys. Chem. Lett.* **2012,** *3*, 1624-1628.
10. (a) Lee, D.; Donkers, R. L.; Wang, G. L.; Harper, A. S.; Murray, R. W. *J. Am. Chem. Soc.* **2004,** *126*, 6193-6199; (b) Jimenez, V. L.; Georganopoulou, D. G.; White, R. J.; Harper, A. S.; Mills, A. J.; Lee, D. I.; Murray, R. W. *Langmuir* **2004,** *20*, 6864-6870; (c) Balasubramanian, R.; Guo, R.; Mills, A. J.; Murray, R. W. *J. Am. Chem. Soc.* **2005,** *127*, 8126-8132; (d) Menard, L. D.; Gao, S. P.; Xu, H. P.; Twesten, R. D.; Harper, A. S.; Song, Y.; Wang, G. L.; Douglas, A. D.; Yang, J. C.; Frenkel, A. I.; Nuzzo, R. G.; Murray, R. W. *J. Phys. Chem. B* **2006,** *110*, 12874-12883; (e) Chen, S. W.; Ingram, R. S.; Hostetler, M. J.; Pietron, J. J.; Murray, R. W.; Schaaff, T. G.; Khoury, J. T.; Alvarez, M. M.; Whetten, R. L. *Science* **1998,** *280*, 2098-2101.
11. Pei, Y.; Zeng, X. C. *Nanoscale* **2012,** *4*, 4054-4072.
12. Tang, Z. H.; Robinson, D. A.; Bokossa, N.; Xu, B.; Wang, S. M.; Wang, G. L. *J. Am. Chem. Soc.* **2011,** *133*, 16037-16044.
13. (a) Garcia-Morales, V.; Mafe, S. *J. Phys. Chem. C* **2007,** *111*, 7242-7250; (b) Su, B.; Zhang, M. Q.; Shao, Y. H.; Girault, H. H. *J. Phys. Chem. B* **2006,** *110*, 21460-21466.
14. Tlahuice-Flores, A.; Santiago, U.; Bahena, D.; Vinogradova, E.; Conroy, C. V.; Ahuja, T.; Bach, S. B. H.; Ponce, A.; Wang, G. L.; Jose-Yacaman, M.; Whetten, R. L. *J. Phys. Chem. A* **2013,** *117*, 10470-10476.
15. Lagrost, C.; Carrie, D.; Vaultier, M.; Hapiot, P. *J. Phys. Chem. A* **2003,** *107*, 745-752.
16. Flanagan, J. B.; Margel, S.; Bard, A. J.; Anson, F. C. *J. Am. Chem. Soc.* **1987,** *100*, 4248-4253.
17. (a) Antonello, S.; Holm, A. H.; Instuli, E.; Maran, F. *J. Am. Chem. Soc.* **2007,** *129*, 9836-9837; (b) Antonello, S.; Perera, N. V.; Ruzzi, M.; Gascon, J. A.; Maran, F. *J. Am. Chem. Soc.* **2013,** *135*, 15585-15594.
18. Alvarez, M. M.; Khoury, J. T.; Schaaff, T. G.; Shafigullin, M. N.; Vezmar, I.; Whetten, R. L. *J. Phys. Chem. B* **1997,** *101*, 3706-3711.